CHEMICAL ENGINEERING TRANSACTIONS
VOL. 43, 2015
A publication of AIDIC
The Italian Association of Chemical Engineering
Online at www.aidic.it/cet
Chief Editors: Sauro Pierucci, Jiří J. Klemeš

ISBN 978-88-95608-34-1; **ISSN** 2283-9216
DOI: 10.3303/CET1543273

Numerical Study of the Impact of the Solution Flow Rate in the Supercritical Antisolvent Process: a 3D Approach

Regiani A. Almeida*[a], Ricardo V. P. Rezende[b], Reginaldo Guirardello[c], Henry F. Meier[d], Dirceu Noriler[d], Lúcio C. Filho[a], Vladimir F. Cabral[a]

[a]Department of Chemical Engineering, State University of Maringa, Maringa 87020-900, Brazil
[b]Department of Chemical Engineering, Federal University of Santa Catarina, Florianopolis 88040-970, Brazil
[c]College of Chemical Engineering, State University of Campinas, Campinas - SP, 13083-852, Brazil.
[d] Department of Chemical Engineering, Regional University of Blumenau, Blumenau 89030-000, Brazil
regiani_al@hotmail.com

Processes for precipitation of micro and nanoparticles using CO_2 in supercritical state have proved to be an efficient way to process a large number of compounds from various fields, particularly in the pharmaceutical and food industry. In the face of experimental difficulties, the computer simulation appears as a useful tool to determine important parameters of the process. Using a three-dimensional mathematical model, it was studied the development of a jet of solution (ethanol and minocycline) expanded in pressurized carbon dioxide in order to interpret the process of development of regions of supersaturation of the solution. The commercial code ANSYS FLUENT was used to solve the model relating the impact of the flow of solution (1, 3 and 5 ml/min) in the mixing chamber of the precipitation process. The influence of turbulence in the flow dynamics was analyzed with the k-ε and k-ω models. Analysis of supersaturation profiles showed that by increasing the solution flow rate there is an increase in supersaturation and also occur more recirculation regions. So the conditions of injection of a given solution, considered in this work, determine distinct regions of nucleation and particle growth. These characteristics can be taken into account in the design of a chamber that offers conditions for the precipitation of small particle with fewer clusters.

1. Introduction

The use of techniques based on Supercritical Fluid (SCF) for the particles precipitation enable the production of a wide variety of pharmaceutical products and foods (Martín et al., 2007). Such particles may exhibit regular shape (spherical) in micro and nanometer scale (Rossmann et al., 2012). In the Supercritical Antisolvent technique (SAS), the precipitation of a solute occurs by considering an organic solution containing the solute of interest diluted in an organic solvent being injected though a capillary tube in a pressurized chamber and loaded with CO_2, which is used as antisolvent for the extraction of the solute from solution (Lengsfeld et al., 2000). There is the development of a jet of fluids at low speeds (with Reynolds numbers of the order of 10^3) (Sierra-Pallares et al., 2012). The variation of the feed flow rate of the solution and of the CO_2 are parameters which directly affect the distribution of supersaturation, and thereby, the morphology and the particle size (Bałdyga et al., 2010).
The precipitation mechanisms using SCF were not systematically studied. There are discrepancies in the literature regarding the impact of changes in operating parameters when considering different systems (solutions) (Fages et al., 2004), and little is known about the behavior of supercritical fluid dynamic mixing and its effect on the size and shape of the crystallized particles (Reverchon et al., 2011).
Experimental evidences shows that the SAS process presents a complex flow pattern due to the way of interaction of high pressure; fast mass transfer; between the solution and the particles extracted by the supercritical CO_2 (Jerzy et al., 2004); and many regions of nucleation and growth of very small particles (Cushen et al., 2012). Numerical simulation is present in several areas of engineering (D'Aulisa et al., 2014).

Please cite this article as: Almeida R.A., Rezende R., Guirardello R., Meier H., Noriler D., Cardozo Filho L., Cabral V., 2015, Numerical study of the impact of the solution flow rate in the supercritical antisolvent process - a 3d approach, Chemical Engineering Transactions, 43, 1633-1638 DOI: 10.3303/CET1543273

To improve understanding of the flow dynamics of the SAS process, some works as Erriguible, Laugier, et al. (2013) have been proposed employing mathematical modeling from the computer simulation using Computational Fluid Dynamic (CFD).
Concerning an increase in inlet flow rate of solution, Cardoso *et al.* (2008) and collaborators, using a incompressible, isothermal regime, indicate that the flow rate of solution has little effect on the average size of the particles, but it plays a role in the size distribution: a narrowing of the size distribution and an increased homogeneity of the precipitated particles were observed. For the same operating conditions that Cardoso et al. (2008) and Erriguible, Fadli, et al. (2013) concluded that the increased inlet flow rate of solution, combined with more concentrated solutions of solute particles result in small and more regular shapes of particles, nevertheless, this methodology requires a large computational effort.
In order to improve understanding of the fluid and particles flow dynamics, the aim of this study is to evaluate the impact of increasing the solution flow rate in the flow pattern and, consequently, in the precipitated particles. For this purpose, it is presented a mathematical model for compressible, non-isothermal turbulent and steady state regime and ANSYS Fluent software was used for its solution.

2. Governing equations

Under the operating conditions (T_{op}= 313 K and p_{op}=130 bar), the antisolvent and the solution containing organic solvent and solute are completely miscible and so the SAS process is operated above the critical point of the mixture (a single phase region). A pressurized CO_2 stream enters from the side of the precipitation chamber the organic solvent + solute stream is injected on the center of the chamber through capillary tube as the work of Cardoso et al. (2008). The chamber configuration and its grid are depicted in Figure 1.
The precipitation process involves nucleation and growth of particles from a supersaturated solution. The supersaturation $\mathbb{S}$ is defined by the Eq. (1), and, according to crystallization kinetics, high supersaturation leads to high nucleation rate (Mullin, 2001):

$$\mathbb{S} = \frac{y_S}{y_{S,eq}}, \tag{1}$$

where y_s is the mass fraction of solute and $y_{s,eq}$ is equilibrium mass fraction of the solute in the mixture: minocycline + ethanol + CO_2, given by the expression $y_{s,eq} = 1\times10^{-5}\exp\left(25.8 y_{ethanol}\right)$ Cardoso et al. (2008).

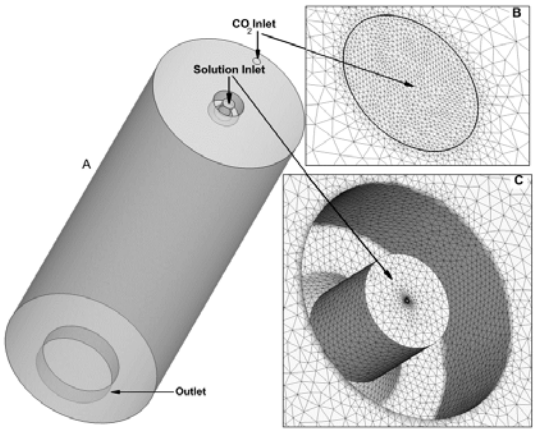

Figure 1: SAS chamber. A) Geometry; B) Mesh details about the CO_2 inlet; Mesh details about the solution Inlet

2.1 Thermodynamic modelling

The compressibility of the mixture is described by the Peng-Robinson state equation with van der Waals quadratic mixing rule (Poling et al., 2004). For the viscosity of the mixture it was employed the $\mu_{mix} = \exp\left(y_2 ln\mu_{Co2} + y_1 ln\mu_{Etanol}\right)$, where the viscosities are: $\mu_{CO_2} = 4.97\times10^{-5}\,Pa.s$ and $\mu_{ethanol} = 0.567\times10^{-3}\,Pa.s$ calculated by means the Chung's method (Chung et al., 1988), y_1 and y_2 are the mass fraction of ethanol and CO_2 respectively. The coefficient of molecular diffusivity is assumed constant $D_m = 1.69\times10^{-8}\,m^2/s$ (Cardoso et al., 2008).

2.2 Transport equations

The supercritical fluid phase is represented by a eulerian framework, where $\overline{\cdot}$ and $\widetilde{\cdot}$ are average Reynolds and the average Favre respectively (Reynolds, 1895; Wilcox, 1993). The eddy viscosity hypothesis is assumed, flow can be analyzed under steady-state compressible. The continuity, momentum, energy and species are given as follows:

$$\partial_i \left(\overline{\rho} \tilde{u}_i \right) = 0 , \tag{2}$$

$$\partial_i \left(\overline{\rho} \tilde{u}_i \tilde{u}_j \right) = \partial_j \overline{P} + \partial_j \left(\tilde{\tau}_{ij} - \overline{\rho} \widetilde{u'_i u'_j} \right), \tag{3}$$

$$\partial_i \left(\overline{\rho} \tilde{u}_i \tilde{h} \right) = \partial_j \left\{ \left[\left(K_m + K_T \right) / c_p \right] \partial_j \tilde{h} \right\} + \tilde{\tau}_{ij} \partial_j \widetilde{u_i} , \tag{4}$$

$$\partial_j \left(\overline{\rho} \tilde{u}_j \tilde{y}_i + \overline{\rho} \widetilde{u_j'' y_i''} \right) = \partial_j \left(\overline{\rho} \left(D_m + D_T \right) \partial_j \widetilde{y_i} \right), \tag{5}$$

where u_i is the component i of the velocity vector, $P = p_{op} + p_{gauge}$ is the static pressure y_i is the mass fraction of component i, $\tilde{\tau}_{ij}$ is the viscous stress tensor and the term, $-\overline{\rho} \widetilde{u'_i u'_j}$ is the Reynolds stress tensor, determined by the turbulence model to two equations. In Eq.(5), $D_T = \mu_T / \overline{\rho} Sh_T$ is turbulent diffusivity of mixture, Sh_T the turbulent number of Schmidt and μ_T, the turbulent viscosity. In Eq. (4) $\tilde{h}$ is the enthalpy, K_m, K_T is the molecular and turbulent thermal conductivity respectively. The *k-ε* and *k-ω* turbulence models are employed to close the set of Eq.(2)-(5) for the unknown terms that emerged after consideration of averages. The complete description and derivation of the transport equation for turbulent kinetic energy *k*, dissipation rate of turbulent kinetic energy *ε*, and specific rate of dissipation *ω* also employed in this study can be found (ANSYS, 2010).

3. Operating conditions and numerical details

The geometry of the chamber is a cylinder as show the Figure 1 (A), which has a volume of 255.2 *ml*; a diameter of CO_2 inlet of 2.5 mm and solution inlet diameter of 0.125 mm. Under 130 bar operating pressure and 313.15 *K* operating temperature. The inlets boundary conditions were mass flow rate in the solution inlet and in the CO_2 inlet. Conditions of turbulence intensity of 1% were considered based on low Reynolds numbers in the inlets and outlets of the camera, in outlet of the chamber was used pressure condition (p_{gauge}= 0 *bar*). Three cases were simulated by varying the solution inlet flow rate: **case 1**: 1 ml / min, **case 2**: 2 ml / min and **case 3**: 5 ml / min, keeping the CO_2 inlet flow rate at 6.56 ml / min. From the geometry in Figure1 (A), was generated a tetrahedral mesh with 1.2×10^6 cells with regions of the refinement in solution and CO_2 inlets as can be seen in Figure 1 (B) and (C). With increasing inlet flow rate, the model becomes difficult to convergence. The *k-ε* and *k-ω* turbulence models were considered in order to evaluate their influence on patterns of flow including case 1 for comparison purposes, as discussed in section 3. From the software ANSYS Fluent 13.0, the pressure-based coupled solver was used and the system of Equations (2)-(5) coupled to the turbulence model. And spatial discretization scheme of the first order were used.

3. Results and Discussion

3.1 Validation of the Model

The opening angle of a turbulent jet deduced from the theory of entrainment of fluid into another is approximately 11.8 degrees and the velocity profile of jet has the shape of a Gaussian curve (Cushman-Roisin, 2013). The opening angle of the jet obtained in this work was approximately 15 degrees for a central cut plane as is depicted in Figure 2 (a) (employing the turbulence model *k-ω*). Moreover, the Gaussian velocity profile and the opening angle of the jet have a good approximation to that described in the theory of jet entrainment.

3.2 Stokes Number

The Stokes number $St = \tau U / d_p$ measures the ratio of the response time of the particle in relation to the characteristic time scale of the flow (τ is the relaxation time of the particle and U / d_p is the characteristic time of the flow). If $St \ll 1$ means that the response time is short and the particle trajectory follows the direction of the flow streamlines of the continuous phase. If $St \gg 1$ means that the particle will follow its own path and

slow to respond to changes in the flow pattern of the continuous phase (Crowe et al., 1998; Rezende, 2013). For all cases simulated in this study the number of Stokes remained less than unity ($St \leq 0.1$) as shown in Figure 2 (b). Thus, the trajectories of the particles follow the streamlines of the flow.

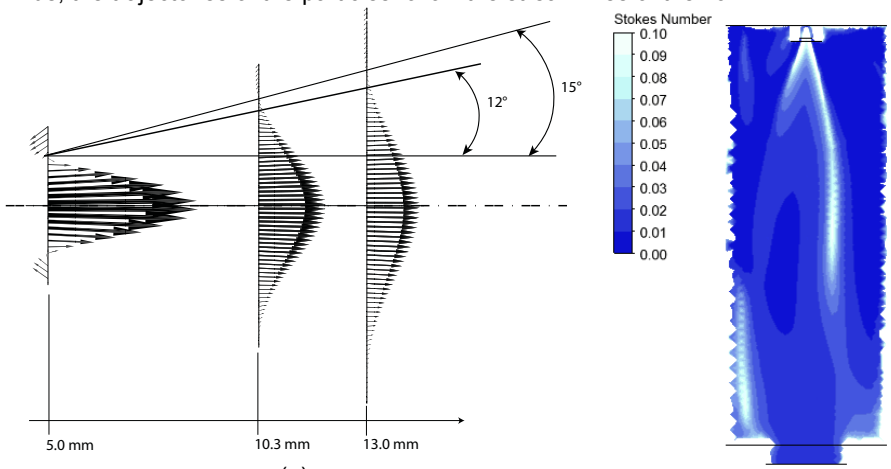

Figure 2: (a) Velocity vectors and opening angle of the jet: 11.8 degrees in literature, 15 degrees in this work; (b) Stokes number for a central cut plan in case 1 with k-ω turbulence model

3.3 Turbulence

The action of the turbulence influences the flow increasing the effective diffusivity, the transport of heat, mass and momentum. The transition from laminar to turbulent regime jets depends on the flow conditions downstream near the outlet solution and the low Reynolds numbers, starting at *Re* = 10 (Drazin et al., 1981). The case 1 (the Reynolds number in inlet of solution is *Re*=140), can be solved in the Fluent software without a turbulence model, but the models of turbulence *k-ε* and *k-ω* were also used and a comparison of the magnitude of the velocity from these modelling approaches in the center line appears in the graph of Figure 3 (a). For the cases 2 and 3, the Reynolds number in the inlets of solution was *Re*=420 and *Re*=700 respectively. In the Figure 3 (b) we observe the opening angle of the jet solution according with the two turbulence models employed. The one who is closer to the angle given by the literature was the *k-ω* model.

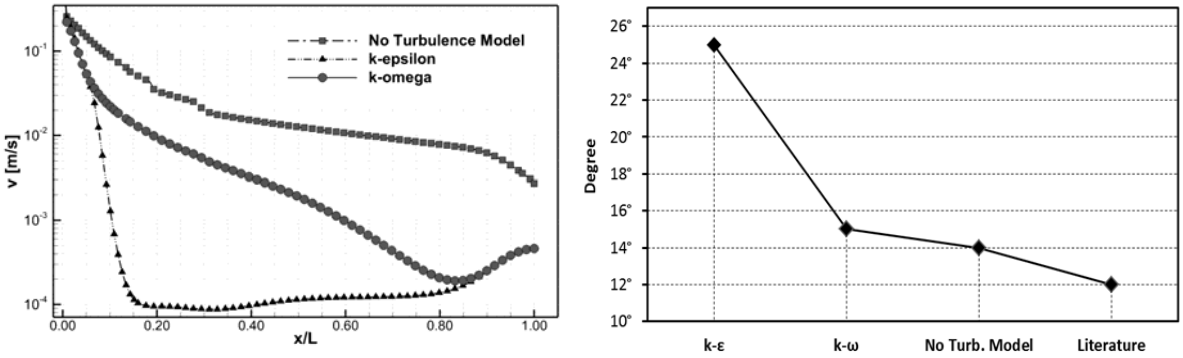

*Figure 3: Impact of the turbulence model for the **case 1** when: no turbulence model was used and when the k-ω and k-ε turbulence models were employed. (a) On magnitude of the velocity in center line of the camera (L is the length of chamber (m)); (b) On the opening angle of the jet solution when compared with the opening angle computed in the literature (Cushman-Roisin, 2013)*

It can be observed in Figure 3 (a) at the center line of the precipitation chamber that the velocity magnitude when employing the *k-ε* model are quite different from the values when employed the *k-ω* model. But with the *k-ε* model the magnitude of the average velocity takes values next to zero in the lower half of the chamber length. For cases 2 and 3 the convergence was achieved only when a turbulence model was employed.

3.4 Supersaturation

The central plans section of chamber in Figure 4 shows that supersaturation increases with increasing the inlet flow rate of solution within the SAS chamber. As the inlet flow rate of the solution increases, there is a bending of the CO_2 towards the solution jet due the entrainment effect. This increases the mixture of the two streams and, consequently, an elevation in the supersaturation is observed. In the cases 2 and 3, with the higher flow rates, more particles recirculation regions are observed. In case 1, supersaturation are better distributed within the chamber, while in case 2, there are high values of supersaturation in the center of the chamber. For case 3, there are high values in a larger volume of the chamber and they occur in areas near the entrance and at the bottom. At a high level of supersaturation, the rate of nucleation is higher and more stable nuclei are generated and the crystal growth phase of the crystallization is more regular. This leads to smaller particles and less formation of secondary structures (clusters and blades) (Rossmann et al., 2012).

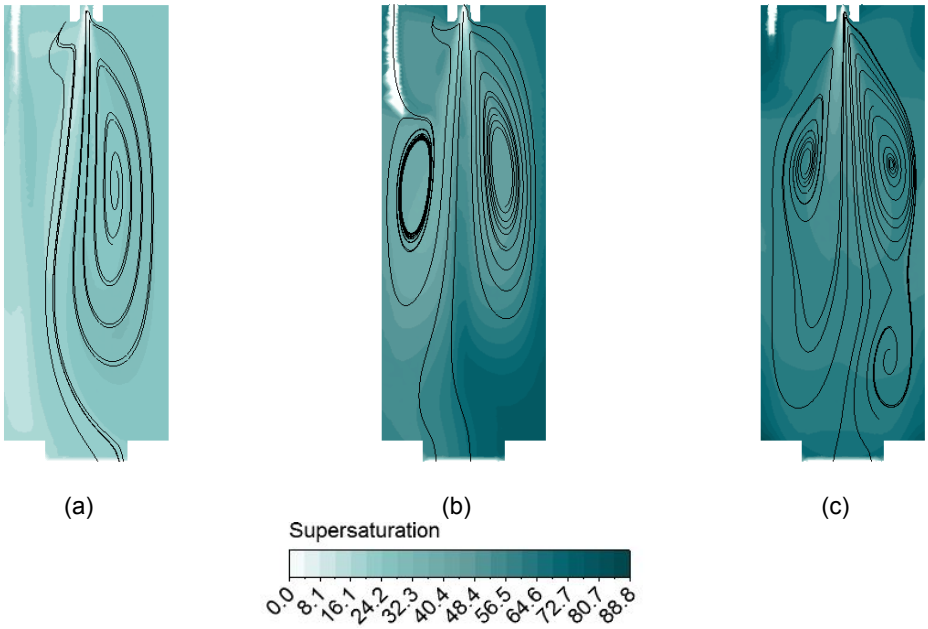

Figure 4: Stream lines and contour map of supersaturation in a central cutting plane of chamber with k-ω turbulence model. (a) Case 1; (b) Case 2; (c) Case 3.

4. Conclusion

The proposed low-cost methodology was able to reproduce the jet pattern flow according to the classical theory and the flow inside of the SAS chamber. The *k-ω* turbulence model seems to be suitable to model the flow, although other operation conditions must be studied. An increase in the solution flow rate played a key role concerning to supersaturation field. Higher solution flow rates causes a better mixture of the CO_2 and the solution due the jet entrainment effect as well as more recirculation zones, which also implies higher supersaturation mean values and a vortex capture of precipitated particles according to Stokes number analyses has shown. These facts indicate that the case 3 presents a better condition, promoting higher nucleation rates and a more uniform morphology. Finally, we point out that in the cases studied, there was a variation of ~7 K in temperature range on average, this can interfere with the density field and this indicates that the model should be solved in non-isothermal regime.

References

ANSYS F. 2010, *ANSYS FLUENT, Inc. User Guide.*

Bałdyga J., Kubicki D., Shekunov B.Y., Smith K.B. 2010, Mixing effects on particle formation in supercritical fluids. Chemical Engineering Research and Design, 88(9), 1131-1141. DOI: dx.doi.org/10.1016/j.cherd.2010.02.016

Cardoso M.A.T., Cabral J.M.S., Palavra A.M.F., Geraldes V. 2008, CFD analysis of supercritical antisolvent (SAS) micronization of minocycline hydrochloride. The Journal of Supercritical Fluids, 47(2), 247-258. DOI: dx.doi.org/10.1016/j.supflu.2008.08.008

Chung T.H., Ajlan M., Lee L.L., Starling K.E. 1988, Generalized multiparameter correlation for nonpolar and polar fluid transport properties. Industrial & Engineering Chemistry Research, 27(4), 671-679. DOI: 10.1021/ie00076a024

Crowe C.T., Schwarzkopf J.D., Sommerfeld M., Tsuji Y. 1998, Multiphase Flows with Droplets and Particles: CRC Press.

Cushen M., Kerry J., Morris M., Cruz-Romero M., Cummins E. 2012, Nanotechnologies in the food industry – Recent developments, risks and regulation. Trends in Food Science & Technology, 24(1), 30-46. DOI: dx.doi.org/10.1016/j.tifs.2011.10.006

Cushman-Roisin B. 2013, Environmental Fluid Mechanics. United States of America: John Wiley & Sons, Inc.

D'Aulisa A., Simone D., Landucci G., Tugnoli A., Cozzani V., Birk M. 2014, Numerical Simulation of Tanks Containing Pressurized Gas Exposed to Accidental Fires: Evaluation of the Transient Heat Up. Chemical Engineering Transactions, 36, 6.

Drazin P.G., Reid W.H. 1981, *Hydrodynamic stability*. New York : Cambridge University Press.

Erriguible A., Fadli T., Subra-Paternault P. 2013, A complete 3D simulation of a crystallization process induced by supercritical CO2 to predict particle size. Computers & Chemical Engineering, 52(0), 1-9. DOI: dx.doi.org/10.1016/j.compchemeng.2012.12.002

Erriguible A., Laugier S., Laté M., Subra-Paternault P. 2013, Effect of pressure and non-isothermal injection on re-crystallization by CO2 antisolvent: Solubility measurements, simulation of mixing and experiments. The Journal of Supercritical Fluids, 76(0), 115-125. DOI: dx.doi.org/10.1016/j.supflu.2013.01.015

Fages J., Lochard H., Letourneau J.-J., Sauceau M., Rodier E. 2004, Particle generation for pharmaceutical applications using supercritical fluid technology. Powder Technology, 141(3), 219-226. DOI: dx.doi.org/10.1016/j.powtec.2004.02.007

Jerzy, Boris S., Marek H., Baldyga. 2004, Fluid Dynamics, Mass Transfer, and Particle Formation in Supercritical Fluids Supercritical Fluid Technology for Drug Product Development: Informa Healthcare.

Lengsfeld C.S., Delplanque J.P., Barocas V.H., Randolph T.W. 2000, Mechanism Governing Microparticle Morphology during Precipitation by a Compressed Antisolvent: Atomization vs Nucleation and Growth. The Journal of Physical Chemistry B, 104(12), 2725-2735. DOI: 10.1021/jp9931511

Marra F., De Marco I., Reverchon E. 2012, Numerical analysis of the characteristic times controlling supercritical antisolvent micronization. Chemical Engineering Science, 71(0), 39-45. DOI: dx.doi.org/10.1016/j.ces.2011.12.019

Martín A., Cocero M.J. 2004, Numerical modeling of jet hydrodynamics, mass transfer, and crystallization kinetics in the supercritical antisolvent (SAS) process. The Journal of Supercritical Fluids, 32(1–3), 203-219. DOI: dx.doi.org/10.1016/j.supflu.2004.02.009

Martín A., Mattea F., Gutiérrez L., Miguel F., Cocero M.J. 2007, Co-precipitation of carotenoids and bio-polymers with the supercritical anti-solvent process. The Journal of Supercritical Fluids, 41(1), 138-147. DOI: dx.doi.org/10.1016/j.supflu.2006.08.009

Mullin J.W. 2001, Crystallization, (Fourth edition ed.). University of London: Butterworth-Heinemann.

Neto A.S. 2002, Simulação de Grandes Escalas de Escoamentos Turbulentos Escola de Primavera de Transição e Turbulência. Turbulência. Rio de Janeiro: ABCM-Associação Brasileira de ciências Mecânicas.

Poling B.E., Prausnitz J.M., O'Connell J.P. 2004, The Properties of Gases and Liquids: McGraw-Hill Companies.

Reverchon E., De Marco I. 2011, Mechanisms controlling supercritical antisolvent precipitate morphology. Chemical Engineering Journal, 169(1–3), 358-370. DOI: dx.doi.org/10.1016/j.cej.2011.02.064

Reynolds O. 1895, On the Dynamical Theory of Incompressible Viscous Fluids and the Determination of the Criterion. Philosophical Transactions of the Royal Society of London. A (1887-1895), 186, 123-164. DOI: dx.doi.org/10.1098/rsta.1895.0004

Rezende R.V.P. 2013, Modelo de Fechamento para o Tensor de Interface no Modelo de Dois Fluidos: Modelagem Matemática e Simulação Numérica, (Doutorado Tese de Doutorao), Universidade Federal de Santa Catarina

Rossmann M., Braeuer A., Dowy S., Gallinger T.G., Leipertz A., Schluecker E. 2012, Solute solubility as criterion for the appearance of amorphous particle precipitation or crystallization in the supercritical antisolvent (SAS) process. The Journal of Supercritical Fluids, 66(0), 350-358. DOI: dx.doi.org/10.1016/j.supflu.2011.11.023

Sierra-Pallares J., Marchisio D.L., Parra-Santos M.T., García-Serna J., Castro F., Cocero M.J. 2012, A computational fluid dynamics study of supercritical antisolvent precipitation: Mixing effects on particle size. AIChE Journal, 58(2), 385-398. DOI: 10.1002/aic.12594

Wilcox D.C. 1993, Turbulence Modeling for CFD La Canada, California DCW Industries.